Energy & Buildings 343 (2025) 115883

Contents lists available at ScienceDirect

Energy & Buildings

journal homepage: www.elsevier.com/locate/enbuild

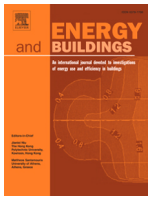

A multi-modal nocturnal radiative cooling and solar-assisted heating system with model predictive control

Manuel Koch [a,b,*], Parantapa Sawant [b], Ralph Eismann [b], Colin N. Jones [a]

[a] EPFL, STI IGM LA3, Lausanne, 1015, Vaud, Switzerland
[b] FHNW, Hofackerstrasse 30, Muttenz, 4132, Basel-Land, Switzerland

ARTICLE INFO

Keywords:
Radiative cooling
Passive cooling
Solar-assisted heating
Building energy systems
Model predictive control

ABSTRACT

Heating and cooling of buildings account for around 15 % of all global energy consumption. In light of the ongoing energy transition, we aim to improve the efficiency of both in a European single-family house by using photovoltaic-thermal collectors with a reversible heat pump for nocturnal radiative cooling, solar-assisted heating and domestic hot water generation. Two data-driven model predictive controllers activate the system during the most favorable ambient conditions for minimal energy consumption. Significant improvements in energy-efficiency of 39.0 % for cooling, 21.7 % for heating and 27.4 % for domestic hot water are achieved over a simulation period of one year, compared to a conventional reference system. We find the building's underfloor radiant slab to be sufficient as a thermal storage for heating and cooling, not requiring a dedicated storage tank. However, a cost estimate indicates long amortization times for the higher installation costs of our proposed multi-energy system. Only the scenario with low-end estimates for the installation costs and high-end estimates for the electricity tariffs reached our target value of less than 20 years.

1. Introduction

Around a third of all primary energy in developed countries is used in buildings, with roughly half of it for heating and cooling, resulting in an estimated 15 % of the total consumption being used for heating and cooling of buildings [1–5]. To supply this consumption, roofs of buildings are increasingly used to generate renewable energy, either with photovoltaics or solar-thermal collectors. Photovoltaic-thermal collectors (PVT) aim to maximize the energy gains by combining both. In this paper, we go one step further in utilizing the roof space, and present a heating and cooling system for a building that combines PVT collectors with a reversible heat pump for nocturnal radiative cooling and solar-assisted heating, while also generating electricity. In a one-year simulation of a single-family house in Central European climate, we show that high efficiency for space heating and cooling, as well as domestic hot water, can be achieved with a compromise design, that is not optimized for any of these individual tasks. Furthermore, we show the feasibility of using an underfloor radiant slab without any additional thermal storage device to provide sufficient cooling during the day, despite only operating the system in cooling-mode at night.

While we assume that the reader is already familiar with photovoltaics and solar-thermal heating, we give a brief introduction to nocturnal radiative cooling: This denotes the physical effect in which an object is cooled by radiative heat exchange with outer space. While the background temperature of outer space is approximately 3 K, this effect is significantly attenuated by the atmosphere, but the radiative sky temperature can still drop well below the ambient air temperature, especially during clear nights[1]. To better illustrate, Fig. 1 shows the spectra of the solar radiation based on [7], the atmospheric transmission[2] based on [8], and the ideal black-body radiation at 25 °C based on Planck's law. The band of high atmospheric transmission between the wavelengths of 8μm to 13μm overlaps significantly with the black-body radiation. Heat emitted at this, or similar, temperature can thus penetrate the atmosphere into outer space well. The radiation spectrum of a real object may deviate from an ideal black-body, but for most common materials, it is a suitable approximation.

We harness this effect by using the PVT collectors as sky-facing radiator surfaces. While the existing literature extensively documents the use of nocturnal radiative cooling for buildings [9–15], they mostly use it in parallel with a conventional cooling system, or for pre-cooling on

[1] This phenomenon can often be observed after a cold night, when cars have a thin layer of ice on their roofs, but not their sides. In ancient Persia, it was used to produce ice in the desert [6].

[2] This data set accounts for scattering at short wavelengths. Without it, the transmission of visible light would be around 90 %.

* Corresponding author.
E-mail address: manuelpascal.koch@epfl.ch; manuel.koch@fhnw.ch (M. Koch).

https://doi.org/10.1016/j.enbuild.2025.115883
Received 9 January 2025; Received in revised form 16 April 2025; Accepted 13 May 2025
Available online 19 May 2025

Nomenclature

A	Area
C	Thermal capacity
I	Radiation
P	Power
T	Temperature
y	Model output
z	Model output
δ	Control variable
θ	Model parameters
φ	Model input
ψ	Model input
ω	Model parameters
CHF	Swiss franc
COP	Coefficient of performance
DHW	Domestic hot water
EER	Energy efficiency ratio
HEX	Heat exchanger
HP	Heat pump
MPC	Model predictive control
PVT	Photovoltaic-thermal
rHP	Reversible heat pump

the external supply-side of a mechanical chiller. Extending the work of [16,17], which only covers cooling, we use the PVT collectors (i.e. radiators) in combination with a reversible heat pump (rHP) and a brine-water heat exchanger (HEX) for a system capable of active and passive heating and cooling. Hereinafter, we refer to this as the "PVT system". Consider Fig. 2 for better understanding: Our PVT system is shown on the left. The only external component are the collectors, which connect to the house through the parallel arrangement of the HEX and rHP. Next to it is a conventional reference system with only a reversible heat pump and an external heat exchanger. The right side shows the aforementioned pre-cooling and parallel configurations, but extended to also cover the heating case, for better comparison. In the pre-cooling (resp. pre-heating) configuration, the PVT collectors are used to pre-condition the working fluid with radiative cooling or solar-thermal heating, before the heat pump brings it to its target temperature. The parallel configuration has two independent sides.

Table 1 compares the properties of the four systems, and highlights the rationale behind our system: Compared to the parallel configuration, we gain the ability of nocturnal radiation-assisted cooling and

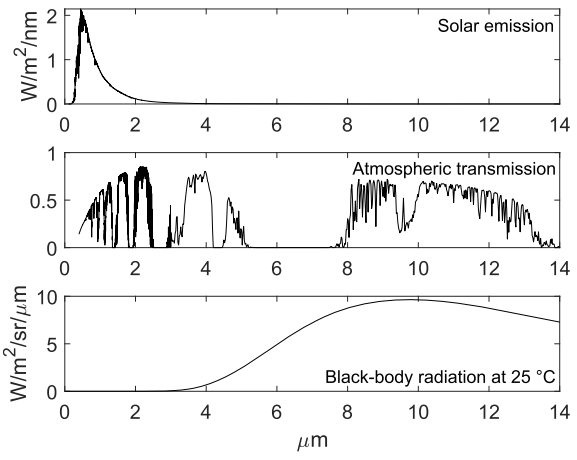

Fig. 1. Spectra of solar emission, atmospheric transmission and ideal black-body radiation at 25 °C at short and medium wavelengths.

solar-assisted heating, meaning that we can still harness some of the benefits of passive heating and cooling when the conditions are insufficient for fully passive operation, which is often the case. While the pre-heating/cooling configuration offers these capabilities as well, our approach has the advantage of fewer components. Namely, the lack of an external fan unit, which makes it inherently compliant with any noise regulations that may apply in a given location, particularly in residential areas [18]. However, this comes at the disadvantage of losing the ability of daytime cooling. Since the necessary conditions for fully passive solar-thermal heating are never reached during our simulations, we omit further reference to it for the remainder of this paper, already having stated the system's fundamental capability.

Because of the aforementioned inability of daytime cooling, we need significant thermal storage capacity to carry the nocturnal cooling power through the following day. Similarly, we want to carry solar-assisted heating power through the following night during the heating season. Rather than using a dedicated storage tank, which would cost money and occupy space, we use the thermal inertia of the building's underfloor radiant slab for this purpose. Because of its thickness, it has a time constant of several hours, making it well-suited for the purpose of load shifting. However, this approach comes with two disadvantages: The time constant of the slab is fixed and may not always match the desired delay. Moreover, avoiding occupant discomfort, and condensation of humid air in the cooling case, imposes a lower limit on the slab temperature. However, the feasibility of using radiant slabs for cooling has been demonstrated before [19,20], including a side-by-side comparison with a forced-air system in a seasonally hot and humid climate [21], which is a particularly challenging scenario for radiant slab cooling.

To address the thermal inertia, and the constraints on temperatures and operating times, we use model predictive control (MPC). This control technique uses a simplified model of the building's thermodynamic properties, in combination with a weather forecast, to calculate a forward-looking series of control inputs, that are optimal under a defined cost function. In our case to minimize the electricity consumption of the system, while maintaining comfortable indoor temperatures. The first step of this optimized series is then executed, before the process is repeated at the next time step, accounting for any deviation of the actual system state from the previously calculated one. Because of the strong synergies between the system side and the control side, we consider the MPC to be an integral part of the PVT system, rather than an extension of it. An appropriately tuned rule-based controller could emulate some of the desirable properties of the MPC, but we do not attempt to implement such a solution in this paper. To avoid the often costly process of obtaining a white-box control model of the building [22,23], we rely on a model identified from measured operational data, the process for which is described in Section 2.2. In addition, the following sections will discuss the simulation model, the formulation of the MPC, and the resulting system performance, compared to a conventional reference, before a discussion of the study's limitations and the conclusions drawn.

2. Methodology

2.1. Simulation model of the building

This section discusses the simulation model, which is almost identical to the one previously used in [17]. It is a modern, well-insulated single-family house with a nominal heating energy consumption of 45 kWh/m²/a, based on [24] and shown in Fig. 3. The building has two storeys with a total usable area of 140 m² and an underfloor radiant slab. Each of the two floors has an area of 70 m², an 8 cm thick concrete radiant slab under the wooden flooring, and is modeled as five nodes. The external brick walls have an area of 221.1 m² and are modeled as four nodes. Solar gains on the faÃ§ade are added to the outermost node. The roof has a total area of 84.1 m² and is modeled as four nodes as well. The furniture and internal walls are jointly modeled as

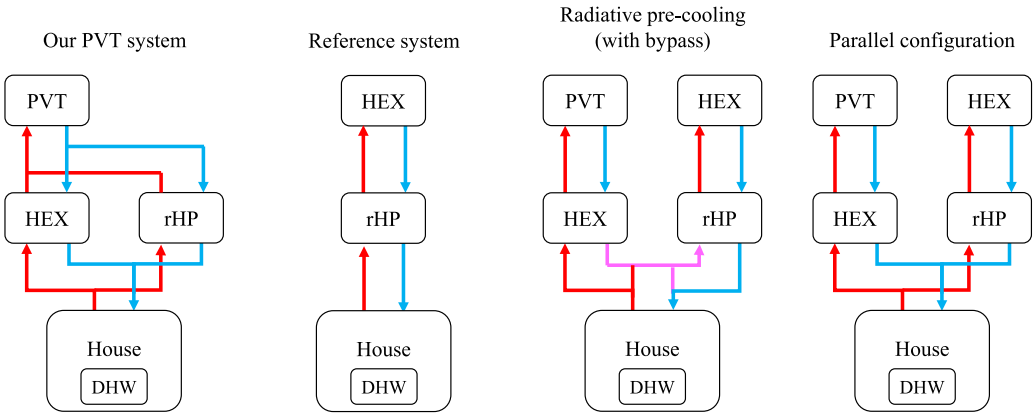

Fig. 2. Hydraulic schematic of our PVT system, the reference system and two alternative system configurations. The line colors (blue for cold, red for hot) are for the cooling case, despite the labels also covering space heating and domestic hot water. (For interpretation of the references to colour in this figure legend, the reader is referred to the web version of this article.)

Table 1
Comparison of different system configurations for nocturnal radiative cooling and solar assisted-heating. ('+': Advantage/capable, '∘': Neutral, '–': Disadvantage/not capable).

	PVT system	Reference	Pre-heating/cooling	Parallel
Silent (no external fan)	+	–	–	–
Fewer components	∘	+	–	–
Daytime cooling	–	+	+	+
Nocturnal radiative cooling	+	–	+	+
Nocturnal radiation- assisted cooling	+	–	+	–
Solar-thermal heating	+	–	+	+
Solar-assisted heating	+	–	+	–

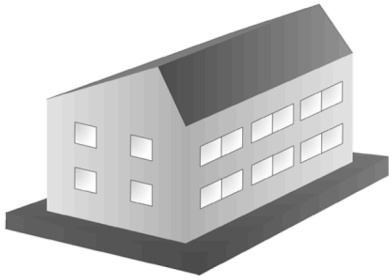

Fig. 3. Drawing of the building model from a north-east angle [24].

200 m^2 of clinker (partially-vitrified fired clay brick) wall, represented by two nodes, as opposed to the single-node representation from [17]. However, this change is found to only have a marginal impact on the results. The inside air measures 389.45 m^3 and is treated as one node. The insulation layers measure 12 cm at the external walls, and 16 cm at the roof and under the ground floor. The ground temperature is modeled as a constant 15 °C. The windows have a total area of 3, 4, 12 and 4 m^2 on the north, east, south and west façades respectively. The heat transfer coefficient is 1.5 $W/m^2/K$, and the G value 0.622. The solar gains are added to the top-layers of the two floors and the outer layer of the internal walls, with the former getting 40 % each and the latter getting 20 %. The convective heat transfer rates on the internal horizontal surfaces are modeled based on [25], while the convective heat transfers on the internal vertical and external surfaces are linearized to constant values based on [25] and [26]. Deviating from the original model, we added a mechanical ventilation with a heat recovery with 60 % efficiency, and automatic shading for the windows. The shading on each side of the house is independently controlled and limits the transmission of the solar radiation to 180 W/m^2, meaning that it is open below the threshold value, then gradually closes as the solar radiation on the corresponding side of the house increases.

The PVT collectors have rear-mounted lamella heat exchangers to increase the convective heat transfer. They cover the entire south-facing side of the roof with an area of 58.8 m^2 and are modeled as one node. The model parameters $\eta_{o,b}$, κ, K_d and a_1 to a_8 of Eq. (1) according *ISO 9806:2017* [27] stem from a commercially available product and are listed in Table 2.

$$\begin{aligned}\dot{q} = {} & \eta_{o,b} K_b(\alpha) I_{col,dir} + \eta_{o,b} K_d I_{col,dif} - a_1(T_{col} - T_{amb}) \\ & - a_2(T_{col} - T_{amb})^2 - a_3 v'(T_{col} - T_{amb}) - a_5 \frac{dT_{col}}{dt} \\ & - a_6 v' I_{col} - a_7 v' \sigma(T_{sky}^4 - T_{col}^4) - a_8(T_{col} - T_{amb})^4 \end{aligned} \quad (1)$$

With $\eta_{o,b}$ the zero loss efficiency, $K_b(\alpha) = 1 - \tan^{\kappa}(\alpha/2)$ the angular dependence for direct solar radiation based on the Ambrosetti function, α the incident angle, $I_{col,dir}$ the direct solar radiation on the collector, K_d the angular dependence for diffuse radiation, $I_{col,dif}$ the diffuse solar radiation on the collector, T_{col} the mean collector temperature, T_{amb} the ambient temperature, $v' = v_{wind} - 3$ m/s the modified wind speed, T_{sky} the radiative sky temperature, σ the Stefan-Boltzmann constant, and I_{col} the total solar radiation on the collector. While the true atmospheric heat exchange is wavelength-dependent, as shown in Fig. 1, it is commonly approximated with an equivalent sky temperature, calculated from ambient conditions, in simulation-based research [11,28–32]. Since the data sheet of the aforementioned product does not include values for the photovoltaics, we assume a typical conversion efficiency of 19 % and 5 % inverter losses. This power is extracted from the thermodynamic balance of the collectors. However, the experimental parameters are determined with the photovoltaics disconnected. We thus adjust the calculation of the thermal power in Eq. (1) by subtracting 19 % from the solar radiation on the collector.

To better convey the properties of the PVT collectors, Fig. 4 shows the cooling power density as a function of the ambient and sky temperature at a constant collector temperature. We assume steady state and a wind speed of 3 m/s. Because of the aforementioned heat exchangers, the cooling power depends more on the ambient temperature than the

Table 2
Experimentally determined model parameters for PVT collectors.

Parameter	Unit	Value
$\eta_{o,b}$		0.402
κ		4.363
K_d		0.887
a_1	$W/m^2/K$	24.988
a_2	$W/m^2/K^2$	0.15
a_3	$Ws/m^3/K$	4.036
a_4		0.058
a_5	$Ws/m^2/K$	6819.4
a_6	s/m	0.032
a_7	s/m	0.083
a_8	$W/m^2/K$	0

sky temperature. However, the latter is still significant for free cooling, when the ambient temperature is only slightly below the collector temperature. Conversely, Fig. 5 shows the heating power density (excluding the electric power from the PV) as a function of the collector temperature and the solar radiation on the collector at a constant ambient and sky temperature. We assume an even split between direct and diffuse radiation. Note that in operation, the collector temperature is strongly coupled to the solar radiation. Therefore, some of the operating points in Fig. 5 may be improbably in practice. Again, we see a high dependence on the difference between the collector and ambient temperature. The importance of this property within the context of the PVT system will be highlighted in Section 3.

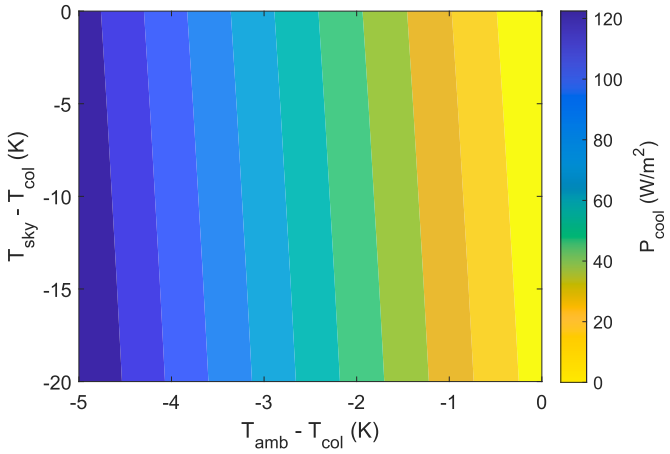

Fig. 4. Cooling power density at $T_{col} = 20\,°C$.

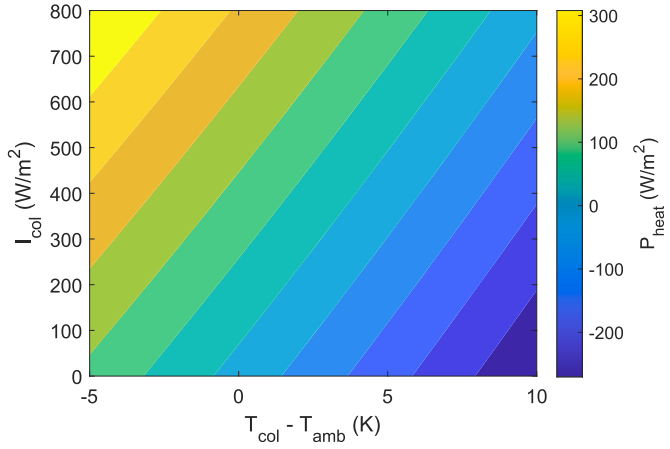

Fig. 5. Heating power density at $T_{amb} = 0\,°C$ and $T_{sky} = -10\,°C$.

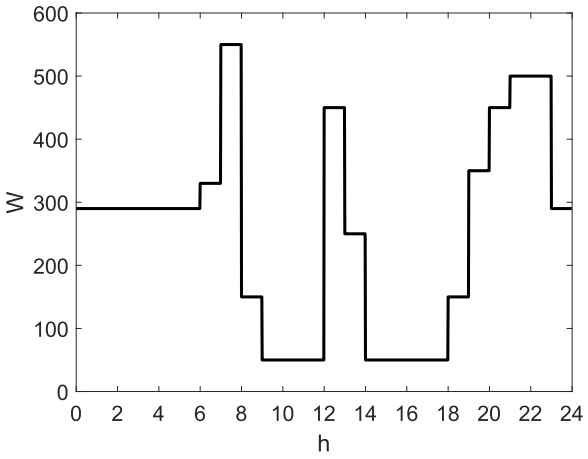

Fig. 6. Daily internal gains profile.

The reversible heat pump has an electric power of 800 W and a nominal coefficient of performance (COP) of 4.0 at a temperature lift of 35 K for heating, which corresponds to an energy efficiency ratio (EER) of 3.0 for cooling at the same temperature lift. The temperature dependence of the COP is modeled as a cropped exponential function (2), with the temperature lift ΔT. This implementation is based on the findings of [33], albeit with adjusted numerical values to be more representative of typical heat pumps using scroll compressors. Comparable efficiency values for very low-lift regimes are reported in [34].

$$COP = max(8,\ 7e^{-0.0242\ \Delta T} + 1) \tag{2}$$

The internal brine-water heat exchanger is modeled based on the number of transfer units (NTU) method. The combined power of the circulation pumps is 100 W, moving 0.13 kg/s of water on the house side and 0.15 kg/s of water-glycol mix with a specific thermal capacity of 3700 J/kg on the external side. The entire system is implemented using Matlab *ode23t*, which is a variable step stiff solver without numerical damping, well-suited for simulating physical systems that have both fast and slow time constants.

We use weather data for Strasbourg, France, [35] which was also assumed for the design of the original model in [24]. Based on a climatological potential analysis for Europe [36], we consider this weather data to be moderately sub-optimal, and thus reasonably challenging to demonstrate the efficiency of the PVT system. The radiative sky temperature is added to the original weather data using the default method of the LBNL *Modelica Buildings Library*, version 8.0.0 [30], relying on the ambient temperature, dew-point temperature and cloud cover. Since there are significant differences between the established models for the calculation of the radiative sky temperature [11,28,37], we perform a corresponding sensitivity analysis in Section 3.2. A repeating daily internal gains profile from [17], shown in Fig. 6, is used, assuming a household with two adults and two children, as well as generally energy-efficient appliances, resulting in an average power of 252.5 W. We note that this profile was originally created for summer. While one may assume some additional gains from lighting during winter, we consider it to be reasonable for both seasons for the purposes of this study.

2.2. System identification

A model $\theta \in \mathbb{R}^{2\times11}$ predicting $y = \begin{pmatrix} T_{zone} & T_{slab} \end{pmatrix}^\top$ is identified, capturing the thermal state of the house in a simplified manner through its zone and slab temperatures. Simplified models with few states have shown similar performance as more complex ones in direct comparison [38]. For reasons detailed in Section 2.3, we choose a long time step of 3600 s for the model, and correspondingly the MPC, but since the building has high thermal inertia, this still captures its dynamics well.

Furthermore, we assume that the slab temperature is being measured. This can be realized by embedding temperature sensors in it, or by maintaining a small flow through the slab's piping and measuring the water temperature at the outlet. The binary control variables are δ_{ca} for the active cooling, δ_{cp} for the passive cooling, and δ_{ha} for the active heating. With T_{amb} the ambient temperature and I_{glo} the global horizontal solar radiation, we get the input (3) at time step k, to predict the next state of the system (4).

$$\varphi_k = (T_{zone},\ T_{slab},\ T_{amb},\ I_{glo},\ \delta_{cp},\ T_{amb}\delta_{cp},\ \delta_{ca},\ T_{amb}\delta_{ca},\ \delta_{ha},\ T_{amb}\delta_{ha},\ I_{glo}\delta_{ha})_k^\top \tag{3}$$

$$y_{k+1} = \theta\varphi_k \tag{4}$$

To motivate this choice of variables, consider the generic mathematical model (5) of a solar-thermal collector, with C_{col} the thermal capacity of the collectors, T_{col} its temperature, $\dot{m}$ the mass flow through it, T_{in} its supply temperature, $H_{col}(v_{wind})$ its wind speed dependent convective heat transfer, A_{col} its area, ε_{col} its overall radiative emissivity, I_{col} the perpendicular solar radiation, σ the Stefan-Boltzmann constant, and ε_{IR} its infrared emissivity. For the identification model, we treat T_{slab} as an approximation of T_{in}, and I_{glo} as an approximation of I_{col}, since the collector orientation is rather flat. The state T_{col} is neglected, since its time constant is fast, compared to the building. After initial trials, T_{sky} and v_{wind} were discarded from the model, because the former is strongly correlated with the ambient temperature, and the latter does not show a significant impact on the output.

$$\begin{aligned} C_{col}\dot{T}_{col} = {} & c_b\dot{m}(T_{in} - T_{col}) + H_{col}(v_{wind})(T_{amb} - T_{col}) \\ & A_{col}\varepsilon_{col}I_{col} + \sigma\varepsilon_{IR}A_{col}(T_{sky}^4 - T_{col}^4) \end{aligned} \tag{5}$$

We collect identification data over a whole year, using simple rule-based control with superimposed randomization. If the zone temperature is below 22 °C, the heating is randomly used with a 75 % probability or not used with a 25 % probability for that day. If the zone temperature is above 23 °C and it is night, the system chooses randomly between doing nothing, active cooling or passive cooling with equal probability for that night. This is a long identification period and the randomized controller results in some constraint violations. It may be possible to obtain a good model of the plant with a shorter or less excited dataset. However, optimizing the system identification procedure is not the focus of this paper. We refer the interested reader to [39,40] for an overview of some alternative methods that may be applied. The identification problem (6) is formulated as a minimization of a Frobenius norm, with $Y = \begin{bmatrix} y_2 & \dots & y_M \end{bmatrix} \in \mathbb{R}^{2\times M-1}$, $\Phi = \begin{bmatrix} \varphi_1 & \dots & \varphi_{M-1} \end{bmatrix} \in \mathbb{R}^{15\times M-1}$, and M the number of samples in the data set. We find that the identified model works well for summer, transient and winter conditions.

$$\min_\theta \|Y - \theta\Phi\|_F^2 \tag{6}$$

2.3. Model predictive control

The MPC (7) is implemented in Gurobi [41], version 10.0.1, and tries to minimize the electricity consumed for heating and cooling the building over a horizon of $N = 24$, i.e. 24 h. It is a mixed-integer problem, which tend to have solving times that grow exponentially with the length of the horizon. Since our system requires day-ahead planning to exploit the day-and-night cycle, the long time step of 3600 s is necessary to keep the solving time within reasonable bounds. The power for passive cooling corresponds to the power of the circulation pumps $P_{pas} = 100$ W. The power for active cooling combines the circulation pumps and the reversible heat pump to $P_{act} = 900$ W. Self-consumption of the PV generation is not considered in the optimization. For the formulation of the control problem, we introduce the shorthand notation $\delta = \begin{pmatrix} \delta_{ca} & \delta_{cp} & \delta_{ha} \end{pmatrix}$ for the binary control variables introduced in Section 2.2. The MPC formulation is completed by the measurement of the current state and the weather forecast (7b), the dynamic constraints (7c), and the state constraints (7d). Eqs. (7f) and (7g) enforce that the cooling is disabled during sunshine, while (7h) enforces that only one mode of operation can be active at a time. Lastly, (7i) to (7k) are a heuristic method to restrict the number of switches each mode can have over the horizon, including the current time step, hence the terms begin one time step in the past. We note that this method does not guarantee to limit the number of switches to the desired upper bound in closed-loop operation. We allow each cooling mode to have one on-off cycle over the horizon, while allowing two for the heating mode. These switching constraints vastly reduce the time to solve the resulting mixed-integer linear program. From a mechanical point of view, reducing the number of switches reduces the wear and tear on the circulation pump, valves and heat pump.

$$\min_{\delta,y} \sum_{k=0}^{N-1} (P_{act}\delta_{ha,k} + P_{act}\delta_{ca,k} + P_{pas}\delta_{cp,k}) \tag{7a}$$

s.t.

$$y_0,\ \delta_{-1},\ T_{amb,[0:N-1]},\ I_{glo,[0:N-1]} \text{ known} \tag{7b}$$

$$y_{k+1} = \theta\varphi_k \tag{7c}$$

$$\begin{pmatrix} 21\,°\text{C} \\ 20\,°\text{C} \end{pmatrix} \le y_k \le \begin{pmatrix} 24.5\,°\text{C} \\ 35\,°\text{C} \end{pmatrix} \tag{7d}$$

$$\delta_k \in \{0,\ 1\}^3 \tag{7e}$$

$$\delta_{ca,k} = 0 \text{ if } I_{glo,k} > 3\,\text{W/m}^2 \tag{7f}$$

$$\delta_{cp,k} = 0 \text{ if } I_{glo,k} > 3\,\text{W/m}^2 \tag{7g}$$

$$\delta_{ha,k} + \delta_{ca,k} + \delta_{cp,k} \le 1 \tag{7h}$$

$$\sum_{j=-1}^{N-1} |\delta_{ha,j+1} - \delta_{ha,j}| \le 4 \tag{7i}$$

$$\sum_{j=-1}^{N-1} |\delta_{ca,j+1} - \delta_{ca,j}| \le 2 \tag{7j}$$

$$\sum_{j=-1}^{N-1} |\delta_{cp,j+1} - \delta_{cp,j}| \le 2 \tag{7k}$$

$$\forall k \in \{0, \dots, N-1\}$$

Since the satisfaction of (7d) cannot be guaranteed, it is actually implemented as a soft constraint. Moreover, the data and model are normalized to a mean of zero and a standard deviation of one. Both are not explicitly expressed in (7) for the sake of legibility. The state constraints are chosen to be (21 °C, 25 °C) for the zone and (20 °C, 35 °C) for the radiant slab, based on [42]. As is expected when using a data-driven model, we observe some inaccuracy over the control horizon. This is particularly relevant for the cooling, which is disabled during the day, thus cannot correct errors until the following night. We account for this by adding an extra safety margin of 0.5 K to the upper zone temperature limit, lowering it to 24.5 °C for the actual optimization.

2.4. Reference system and control

We compare the PVT system to a conventional heating and cooling system, using the same reversible heat pump (2), but with an external air-brine heat exchanger unit with a fan power of 200 W, instead of the PVT collectors. This corresponds to the system shown on the center-left of Fig. 2. A rule-based controller with the switching temperatures 21 °C and 22 °C for heating, and 24 °C and 25 °C for cooling is used. This represents a typical heating and cooling system for residential buildings.

2.5. Domestic hot water

For the sake of a simpler analysis, we investigate the PVT system's efficiency in providing domestic hot water (DHW) separately. The

methodology is essentially a simplified version of the one for the building, hence, we only provide a brief description of the simulation model, system identification, input data and MPC in this section. The same simulated components described above are used to charge a 600 L hot water tank, modeled as one state. The capacity is on the larger side for a single-family house, to better enable the system to utilize the hours with the most favorable ambient conditions, but still much smaller than the stratified storage tanks often used for solar-thermal heating systems, which can be well over 1000 L. A stochastic DHW profile with an average thermal consumption of 6.97 kWh/d was generated using [43]. We multiplied the generated mass flow profile with a constant $\Delta T = 40$ K to obtain a thermal power profile. This results in high peak powers of up to 35 kW. As will be shown in Section 3.3, these peaks deplete the storage tank faster than it can be recharged, resulting in the water temperature dropping significantly below the lower limit. Real human occupants would arguably halt their hot water consumption in this case, but for the scope of this paper, we consider it an acceptable simplification to neglect this. Because the DHW tank shows faster dynamics than the building, a shorter time step for the MPC of 900 s is used.

Since the PVT system cannot reach the necessary temperatures for DHW passively, we only consider the active solar-assisted heating mode. This simplifies the input vector to (8), introducing the storage tank temperature T_{dhw}, the DHW consumption power P_{dhw} and control variable δ_{dhw}. To avoid confusion with Sections 2.2 and 2.3, we introduce new terminology with the output z, the model ω and the inputs ψ in (9). Just as with the building, the system identification and evaluation periods each cover a whole year. The regular charging and discharging of the tank is already well-excited, so no dedicated system identification procedure is necessary.

$$\psi_k = (T_{dhw},\ P_{dhw},\ \delta_{dhw},\ T_{amb}\delta_{dhw},\ I_{glo}\delta_{dhw})_k^\top \tag{8}$$

$$z_{k+1} = \omega\psi_k \tag{9}$$

Because the highest peaks in DHW consumption tend to occur in the morning, and we want to utilize solar-assisted heating during the sunny afternoon hours of the previous day, we use a horizon of 24 h, i.e. $N = 96$, for the MPC (10). For the reasons already mentioned in Section 2.3, this long horizon results in excessive solving times. Since the short time step is forced by the time constants of the system, we implement a work-around and split the control vector into a binary and a continuous component $\delta_{dhw} = \begin{pmatrix}\delta_{bin}^\top & \delta_{con}^\top\end{pmatrix}^\top$. The binary component has a horizon of $N_{bin} = 24$ and is constrained by (10g), allowing two switches during the first 6 h of the total horizon. The continuous component is constrained by (10e). This relaxed reformulation increases the solving speed significantly. The MPC is completed by a cost function minimizing the electricity consumption,[3] the dynamics in (10c), and the state constrains (10d). The forecast $\hat{P}_{dhw}$ in (10b) is based on a looped averaged daily consumption profile. Similar to the MPC in (7), the normalization and the implementation of (10d) as a soft constraint are omitted for legibility. Just as with the building, the reference system in Fig. 2 in combination with a rule-based controller with the same temperature limits is used for comparison.

$$\min_{\delta_{dhw},y} \sum_{k=0}^{N-1} \delta_{dhw} \tag{10a}$$

s.t.

$$z_0,\ \delta_{dhw,-1},\ \hat{P}_{dhw,[0:N-1]},\ T_{amb,[0:N-1]},\ I_{glo,[0:N-1]} \text{ known} \tag{10b}$$

$$z_{k+1} = \omega\psi_k \tag{10c}$$

$$45\,°\text{C} \le z_k \le 55\,°\text{C} \tag{10d}$$

$$0 \le \delta_{con,k} \le 1 \tag{10e}$$

$$\delta_{bin,k} \in \{0,\ 1\} \tag{10f}$$

$$\sum_{j=-1}^{N_{bin}-1} |\delta_{bin,j+1} - \delta_{bin,j}| \le 2 \tag{10g}$$

$$\forall k \in \{0, \dots, N-1\}$$

[3] Since the electric power is proportional to the one-dimensional δ_{dhw}, we can omit the numerical value of the power.

Table 3
Energy use and electricity generation, compared to the reference system. ('Elec.': Electric. 'Ther.': Thermal).

		Cooling			Heating			PV
		Elec. kWh	Ther. kWh	EER	Elec. kWh	Ther. kWh	COP	kWh
Reference		385.0	1869.2	4.86	1965.7	7040.8	3.58	
	Active	209.7	1263.4	6.02				
	Passive	25.2	697.6	27.68				
PVT system	Total	234.9	1961.0	8.35	1539.3	6915.1	4.49	15,944

Table 4
Zone and slab temperature constraint violations in Kelvin-hours, compared to the reference system.

	T_{zone}^{up}	T_{zone}^{low}	T_{slab}^{up}	T_{slab}^{low}
Reference	6.6	41.2	0	0.3
PVT system	0	25.9	0	3.6

3. Results

3.1. Building

Over the evaluation period of one year, summarized in Tables 3 and 4, we find that the PVT system requires 39.0 % less electric energy for cooling and 21.7 % less for heating, compared to the reference, saving a total of 576.5 kW h, while generating 15.9 MW h of electricity from the photovoltaics. Two factors contributing to the lower energy consumption are the operation during favorable ambient conditions, and the lack of an external fan in the PVT system. The PVT system supplies 4.9 % more thermal cooling energy, which can be explained with the losses caused by the need to cool several hours ahead of time. The energy efficiency ratio (EER) is increased by 71.8 %, partially due to the passive cooling mode, which contributes 35.6 % of the cooling energy while only consuming 10.7 % of the electricity. The coefficient of performance (COP) of the heating, which does not use the passive mode, is increased by 25.4 %. Only small violations of the comfort constraints of a few Kelvin-hours over one year are found with either system. The average time to solve the MPC problem on an eight-core *Intel Core i9-11900K* processor is 0.32 s and the maximum 7.70 s. This is fast, relative to the 3600 s time step, but it could take significantly longer on a cheaper processor one might prefer to deploy to control one small building [44].

Fig. 7 shows five days of operation with the PVT system during summer. The zone temperature with the reference system is added for comparison. The two temperature profiles look similar, which is unsurprising, considering they are strongly influenced by internal and ambient gains, which are identical for both simulations. The changes in zone temperature over one day fall into a band of around 1.5 K, which should not cause the occupants thermal discomfort from rapid temperature changes. Fig. 8 shows five days of winter data. The daily zone temperature changes are even smaller with around 1 K.

Fig. 9 provides some insights into the different operation of heating and cooling with the PVT and reference systems. Unsurprisingly, the top plot shows that the predictive and weather-aware controller of the PVT system only activates the cooling at night. Active cooling often occurs right after dusk and right before dawn. The first can be explained by an immediate need to cool during particularly hot days, the second by a need to boost insufficient passive cooling before the system

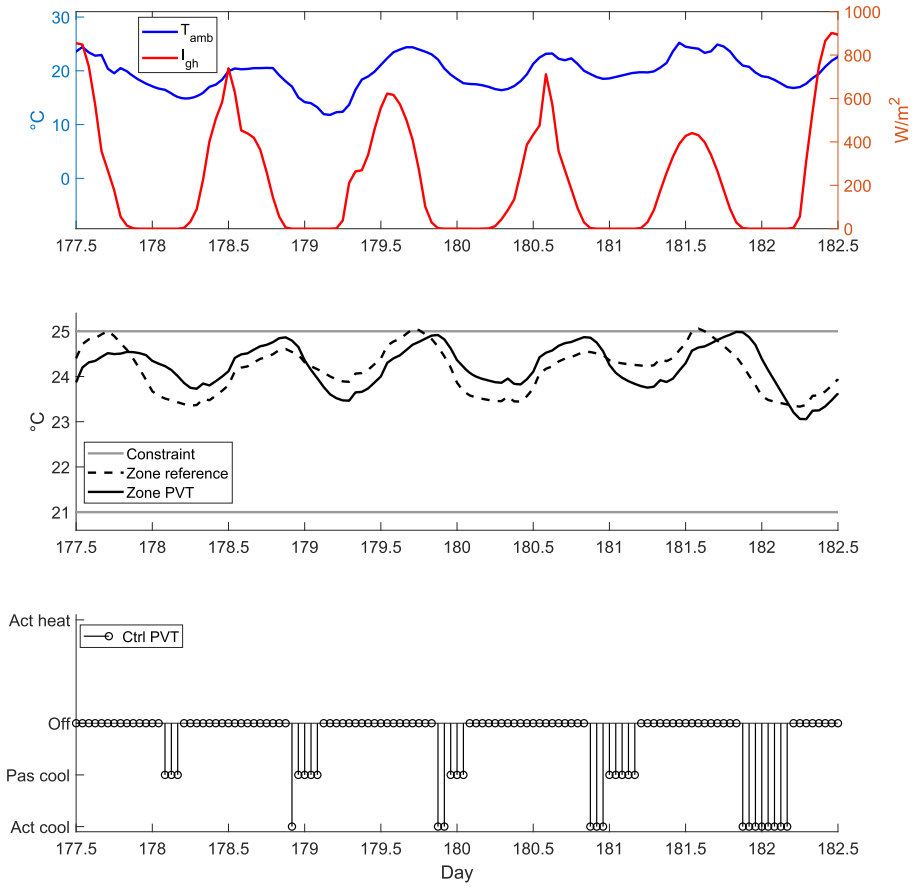

Fig. 7. Time-series of PVT system during summer. Top: Ambient temperature and global horizontal radiation. Middle: Zone temperature and constraints, with reference system for comparison. Bottom: Control.

becomes disabled by the sunrise. The passive cooling is most often active during the middle of the night around 02:00 to 05:00, after the ambient air has significantly cooled down. Incidentally, the rule-based controller of the reference system also mostly activates the cooling during the favorable nightly hours. This is an incidental result of the thermal characteristics of the building and the weather, and is not intentionally induced by our control design choices. However, it does benefit the energy efficiency of the reference system, shown in Table 3, and arguably highlights the efficiency of the PVT system even more. Conversely, the bottom plot compares the activation patterns for the heating. The PVT system is most often activated during the sunny afternoon hours, but also during the early morning hours, when the ambient temperature is at its lowest. This may be caused by the MPC slightly underestimating the temperature loss during the night. Similar to the cooling, the reference system incidentally activates the heating mostly during favorable hours as well. The above point about how this further highlights the efficiency of the PVT system applies again. Unintended by us, the simple reference method happens to behave in a way beneficial to its own efficiency, rather than a more random way, which is what we would have expected.

To isolate the behavior of the PVT collectors in operation, Fig. 10 shows the cooling power density (measured at the heat pump) and collector temperature (measured at the return) for active and passive operation as a function of ambient and sky temperature. Calling back to Fig. 4, we see a stronger correlation with the ambient temperature. While the passive cooling power strongly depends on the ambient conditions, the active cooling power is dominated by the temperature lift from the heat pump, whose power limit causes the ceiling in the cooling power in the top plots. Overall, we find a passive cooling power density for the PVT collectors of up to 100 W/m^2, which is in line with experimental findings from a comparable system in Madrid [28]. Furthermore, review papers covering a wide range of technologies and situations [9,12,13], more or less similar to our setting, report thermal power densities overwhelmingly in line with our results. Fig. 11 shows the heating power density and collector temperature as a function of the ambient temperature and global horizontal radiation. Again, we see a strong dependence on the ambient temperature, because the PVT collectors act as a heat exchanger for the heat pump as much as they are a solar-thermal device.

3.2. Sensitivity to sky temperature modeling

The largest uncertainty in the thermodynamic modeling methodology is arguably the calculation of the radiative sky temperature. While we rely on a well-established building simulation library for this purpose, a review of various calculation methods finds deviations of -19% to +28% from a chosen reference for cooling in temperate climate [37]. To estimate the impact of a potential bias in the calculation of the sky temperature, Table 5 provides a sensitivity analysis of the cooling performance as a function of fixed offsets added to the default weather dataset, detailed in Section 2.1. Regarding the respective shares of active and passive cooling, we note that the default results are a bit of an outlier, compared to the consistent pattern found for the variations. Since the control system is based on a non-convex optimization problem, finding local minima or maxima for a parameter variation is not particularly surprising. Looking at the EERs, we find a consistent pattern

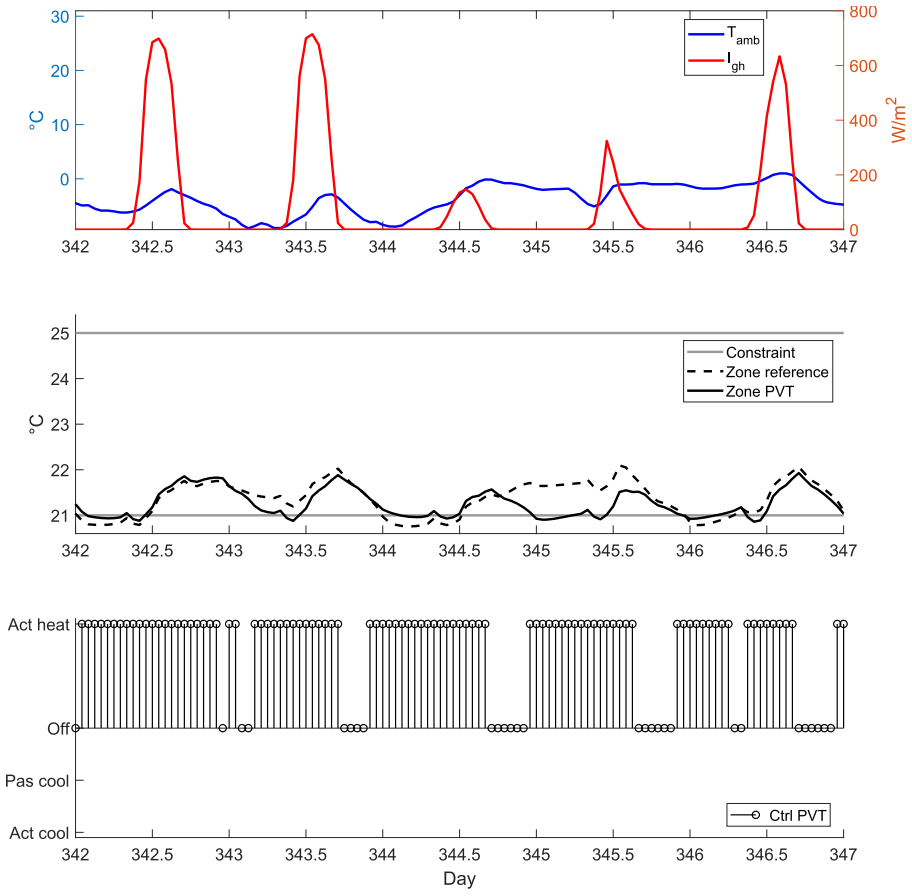

Fig. 8. Time-series of PVT system during winter. Top: Ambient temperature and global horizontal radiation. Middle: Zone temperature and constraints, with reference system for comparison. Bottom: Control.

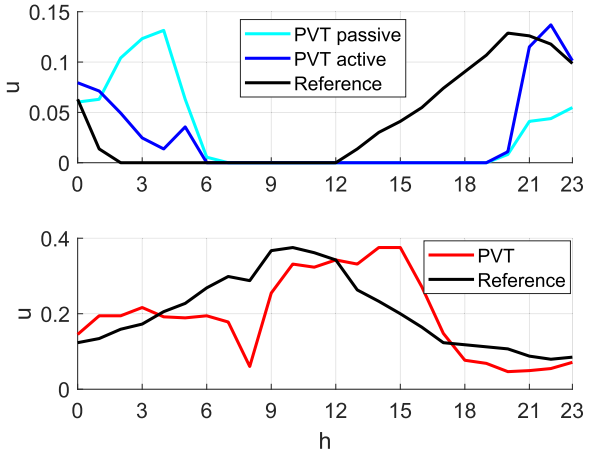

Fig. 9. Top: Averaged daily control action for cooling with the PVT system and the reference. Bottom: Averaged daily control action for heating with the PVT system and the reference.

for all variants. As expected, a lower sky temperature improves the efficiency significantly for passive cooling, but only marginally for active cooling, which is more dominated by convective heat transfer. Varying the sky temperature over a band of 20 K only changes the total energy consumption for cooling by 5 %. We thus conclude that our general findings are robust with respect to uncertainty in the modeling of the sky temperature.

3.3. Domestic hot water

For the generation of DHW over one year, Table 6 shows a reduction of the electricity consumption of 27.4 % with the PVT system, compared to the reference. The total constraint violations, clearly visible in the ten-day extract of operation data in Fig. 12, are higher with the PVT system, but are barely above 1 K h per day on average, which we consider to be acceptable. This is likely caused by the inherent inaccuracy of the consumption forecast, combined with the 900 s time step of the MPC, which sometimes causes a delay in correcting to a prediction error, compared to the quicker response of the reference controller. We further note that if we combine the results for the building and DHW, the PVT system is a net producer of electricity, with the generation being more than six times higher than the consumption. However, taking the domestic electricity consumption into account would significantly reduce this ratio.

Table 5
Sensitivity of cooling performance to offsets of the radiative sky temperature. ('Elec.': Electric. 'Ther.': Thermal).

	Passive			Active		
	Elec. kWh	Ther. kWh	EER	Elec. kWh	Ther. kWh	EER
T_{sky} + 10 K	26.8	717.0	26.76	208.8	1250.6	5.99
T_{sky} + 5 K	26.9	730.3	27.15	205.2	1232.3	6.01
Default	25.2	697.6	27.68	209.7	1263.4	6.02
T_{sky} − 5 K	25.8	733.5	28.43	203.4	1226.1	6.03
T_{sky} − 10 K	26.9	774.5	28.79	197.1	1189.8	6.04

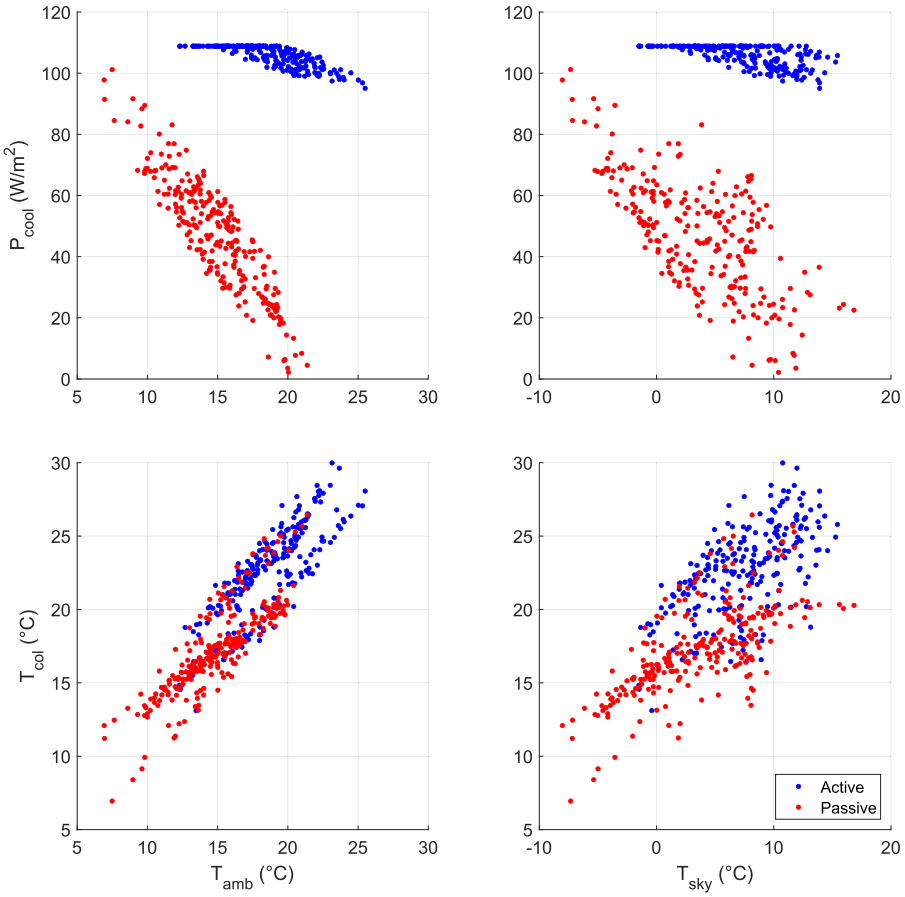

Fig. 10. Cooling power density and collector temperature for active and passive operation as a function of ambient and sky temperature.

Table 6
Energy use and lower temperature limit violation for DHW.

	Electric kWh	Thermal kWh	COP	T_{viol} Kh
Reference	940.8	2505.4	2.66	354.7
PVT system	683.1	2500.4	3.66	437.8

A comparison of the two trajectories in the bottom plot in Fig. 13 shows the impact of the predictive solar-assisted heating. The MPC activates more often during the sunny afternoon hours in anticipation of the significant consumption peak the next morning. Moreover, the recharging after the quick depletion of the storage tank in the morning starts as soon as the consumption increases, as opposed to the purely reactive response of the reference system. The average solving time for the MPC is 0.10 s with a maximum 1.11 s.

3.4. Cost estimate

In this section, we compare the higher costs of the PVT system to the expected energy savings. Based on our experience and consultation with industrial partners, we give a high and low estimate for a number of upfront and ongoing expenses, listed in Table 7. Some components assumed to cost the same for both systems are omitted. The most significant items on the list are PVT collectors and their installation. The external, fan-powered heat exchanger unit of the reference system is more expensive than the internal, passive heat exchanger of the PVT system, but not enough to offset the costs of the PVT collectors. Furthermore, the PVT system requires more piping, as well as four actuated three-way valves, which incurs additional material and installation costs. For the controllers, we assume a small single-board computer for the MPC, and a generic low-cost chip for the rule-based controller, which requires very little computation. The MPC also requires a weather forecast, for which we assume an annual subscription fee. The range of electricity tariffs is oriented on the prices currently found in Switzerland,[4] but with an additional increase on the upper end, in anticipation of such increases in the future. We further assume the tariffs for electricity consumption and feed-in to be coupled, i.e. both to be either high or low.

Combining these cost assumptions with the results of the above sections, we calculate the amortization time for nine scenarios in Table 8, using high, low and geometric mean values for both the electricity and system costs. Based on some assumptions about the longevity of the installed components, we set a target amortization time of no more than 20 years, which is only reached for the high-end estimate of the electricity tariffs combined with the low-end estimate of the system costs. The combination of high electricity tariffs and mean system costs narrowly misses the threshold.

4. Discussion

While we consider the simulation to be reasonably detailed, we will discuss some of the implemented simplifications in the following: Thermal elements with complex geometries are split into one-dimensional layers and represented by strings of thermal nodes. Even if the total thermal capacity and conductivity matches the real object, the selection of the nodes influences the thermal activation, particularly for surface layers. We mitigate this by avoiding layers with high thermal capacity

[4] On the 25th of February, 2025, the exchange rate according to *Google Finance* is 1 CHF = 1.11 USD = 1.07 EUR.

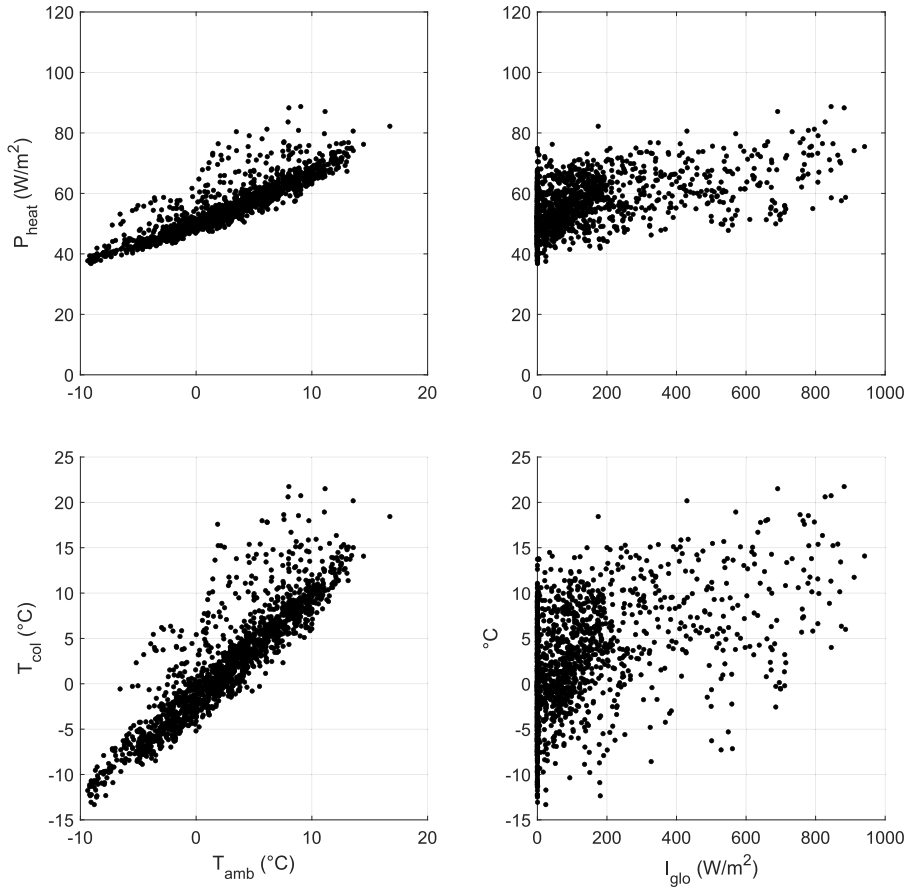

Fig. 11. Heating power density and collector temperature as a function of ambient temperature and solar radiation.

Table 7
Estimated component costs for both systems.

	Details	Unit	PVT system	Reference
PVT	58.8 m^2 total	CHF	25,000–35,000	
Internal HEX	5 kW thermal $\Delta T = 2$ K	CHF	1000 - 1500	
External HEX	7 kW thermal	CHF		3000–4000
Reversible HP	7 kW thermal	CHF	7000–8000	7000–8000
Piping		CHF	2000–3000	1500–2500
Additional valves and actuators		CHF	1200–2400	
Installation		CHF	10,000–20,000	5000–10,000
Control hardware		CHF	100–300	10–30
Weather forecast		CHF/a	100–250	
Electricity cost	PVT: 2457 kW h Ref: 3292 kW h	CHF/kWh	0.25–0.40	0.25–0.40
PV generation	15 944 kW h	CHF/kWh	0.05–0.10	

Table 8
Amortization times for PVT system in years assuming low, geometric mean and high estimates for system and electricity costs.

		System		
		Low	Mean	High
Electricity	**Low**	32.9	43.4	60.4
	Mean	23.1	29.8	40.0
	High	16.3	20.8	27.2

in direct contact with the air. Similarly, the indoor air is represented by one node, neglecting stratification. The internal gains are a fixed, repeating pattern, without any of the random behaviors real humans in a building may display, like opening windows or placing an unintended source of heat near the thermostat. These simplifications are implemented because they lower the computational requirements without significantly impacting the accuracy, or because a more realistic implementation would depend on parameters with high uncertainty. Similar methodologies are used in professional building simulation tools [31,45,46].

Since the same building and DHW models are used for the PVT and reference systems, and the HVAC components that differ are modeled in a comparable manner, we do not believe that the aforementioned points introduce an inherent bias regarding the results and conclusions. One exception to this is the ideal weather forecast, which may benefit the predictive control of the PVT system to some extent. However, the use of ideal weather forecasts is a common practice in simulation-based studies on MPC for buildings [47–49]. To forecast the DHW consumption, we use a simple, non-ideal method based on averaged daily consumption. More advanced methods exist [50,51], but are omitted for the scope of this paper.

Sections 2.2 and 2.3 already mention the inaccuracies of the identified model. While this is nothing unusual in system identification, it

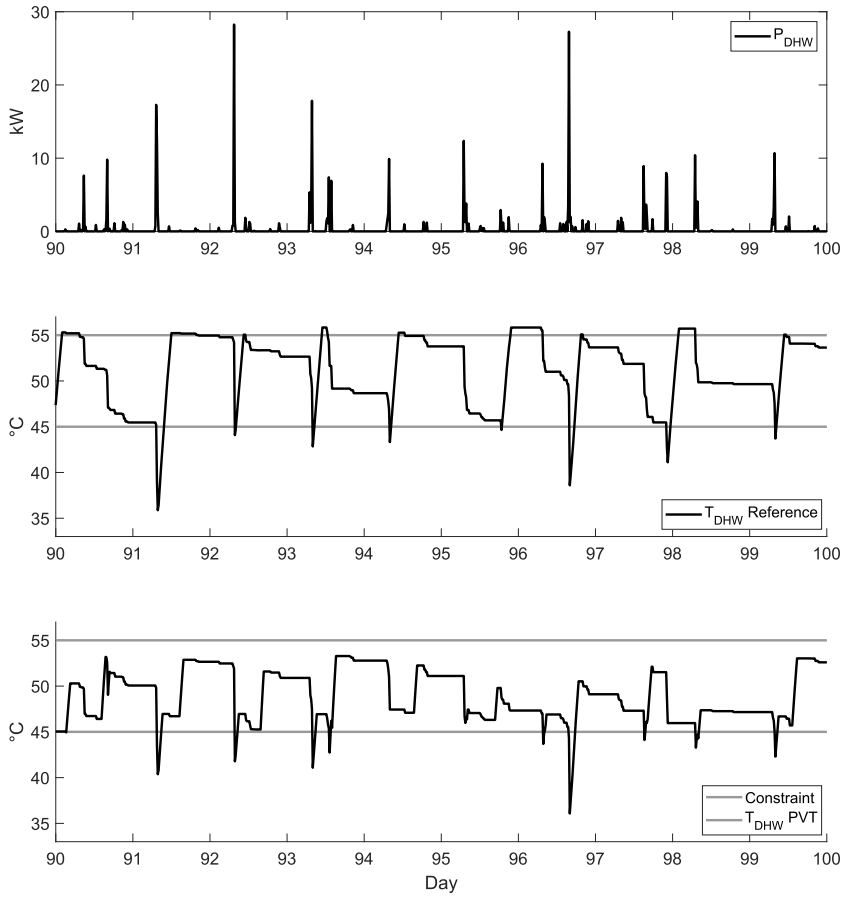

Fig. 12. Ten days of DHW operation. Top: Load profile. Middle: Tank temperature with reference system and rule-based control. Bottom: Tank temperature with PVT system and MPC.

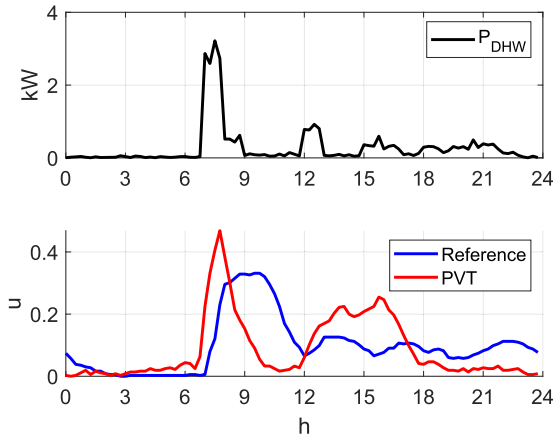

Fig. 13. Top: Averaged daily power of DHW consumption. Bottom: Averaged daily control action with the MPC-controlled PVT system and the rule-based reference.

may have a disproportionate impact on the nocturnal cooling, because the corresponding control action happens ahead of time without the possibility of corrections during the day. A more accurate model might improve the control performance, but since the relationship between model accuracy and control performance in MPC is complicated, we refrain from making any predictions about the practical impact thereof at this point. If minimizing the computational requirements of the MPC is not a high priority, the use of a stochastic model should be considered. This could replace the heuristic safety margin on the upper zone temperature constraint, mentioned in Section 2.3, and result in a more optimal cooling performance, especially if correlations between the degree of inaccuracy and any input values were found, which would enable a dynamic safety margin. Stochastic MPC has been applied to buildings before, including classical parametric [52] and more recent non-parametric [53] approaches, but to the best of our knowledge not with an HVAC system similar to ours.

Despite the benefits shown in this paper, the PVT system also has two fundamental disadvantages, compared to a conventional heating and cooling system: The first one is the low power density of the nocturnal cooling and the resulting high surface area requirement. While the heat pump-assisted active cooling mode substantially mitigates this problem, the PVT system is still much larger than a conventional air-source system, which makes it best suited for buildings with a high ratio of roof to floor area. The second one is the higher installation costs, detailed in Section 3.4. Regarding this cost estimate, we used a simple calculation method and rough estimates, based on our practical experience in our specific location. While we find the costs of the PVT system to be too high for most of the scenarios in Table 8, the balance may be different elsewhere. Since our expertise in this regard is limited to Switzerland, we leave it to the reader to substitute their own local prices, if desired. We believe that the most likely scenario for improved cost-effectiveness is a substantial increase in electricity tariffs. Nevertheless, we propose three possibilities to lower the cost of building the system: (1) The largest item in our cost estimate is the purchase of the PVT collectors, which are a niche technology with low production volume. In contrast, the cost of conventional PV panels has seen an exponential decrease, as production has increased [54]. While we do not expect the production volume of PVT collectors to ever come close to

that of conventional PV panels, even a moderate decrease of their unit cost could significantly improve the expected amortization time. (2) The second biggest cost item is the installation of the PVT collectors. Since we do not expect the salaries of roofers and electricians to decrease, the most promising approach appears to be a partially pre-fabricated installation system, to which the collectors would be attached, and that would simultaneously enforce the statics of the roof to carry the additional weight, in order to enable a faster installation. Modular building systems have been introduced to lower construction costs in the past [55]. (3) We assume a small industrial computer to execute the MPC on location. Depending on the desired level of data privacy, and assuming the building has an internet connection, a cloud-based solution may be cheaper. This cost item is of low significance, compared to the previous two.

Lastly, we note here that buildings and HVAC systems are designed for the climate in which they are located, and for an intended use. In our case a residential building in temperate climate. Evaluating our methods under different conditions, such as a hotter climate or an office building, would thus require a different, appropriately designed building, which is outside of the scope of this paper, and would merit its own study. However, an estimate of how the system would perform in different climates can be derived from the properties of the collectors stated in Section 2.1 and the performance reported in Section 3.1. Moving toward a colder climate, the required cooling would soon drop to insignificant levels, or it could be provided by free cooling with cold ambient air. The COP for heating would decrease from lower source temperatures for the heat pump. In the likely case that the colder climate zone is located further from the equator, the lower solar radiation would add to this. Moving toward a warmer climate, the opposite thereof would apply for the heating case. Regarding the cooling case, in a warm and humid climate, we infer from Figs. 4 and 10 that the contribution of radiative cooling would likely become insignificant, because of the lower atmospheric transmissivity, and because the higher cooling load would require active cooling most of the time. For a hot and dry climate, arguably the most interesting case, the cooling efficiency would benefit from a low nocturnal sky temperature. This may be offset by a higher ambient temperature, depending on how quickly the temperature drops after sunset[5] On the other hand, the cooling load during the day would also be very high under these conditions. If the overall conditions are still favorable for nocturnal cooling, one may consider to increase the thermal storage capacity by installing radiant slabs on the floor and the ceiling, which would also increase the day-time cooling power by doubling the heat exchange surface. Moreover, the convective heat transfer rate is higher when cooling from above, therefore, the achievable cooling power would likely more than double, compared to an underfloor radiant slab alone.

5. Conclusion

A simulation-based evaluation of a novel PVT-based heating and cooling system for a single-family house in Central European climate shows significant reductions of the electricity consumption of 39.0 % for cooling, 21.7 % for heating and 27.4 % for DHW, when compared to a conventional reference system, without sacrificing thermal comfort. We find the serial connection of the heat pump and the PVT collectors to be effective at mitigating the problem of low power density commonly found with nocturnal radiative cooling, showing a high EER for active as well as passive operation. Using the system for heating and cooling required compromises in its design, rather than optimizing it for one of these tasks. This proved to be little hindrance, achieving good performance for either one. We further find the thermal capacity of the radiant slab to be sufficient to maintain a comfortable indoor temperature throughout a summer day, while being restricted to nocturnal cooling, for the given building. Two separate mixed-integer linear MPC formulations using data-driven models, one for heating and cooling, and one for DHW, are shown to solve quickly and reliably. Both make use of constraints and relaxations tailored to their respective applications to accelerate the optimization, compared to a more straight-forward implementation. A cost estimate with multiple scenarios indicates that the higher installation costs of the PVT system can be recuperated by its lower electricity consumption in less than 20 years, but only for the scenario with high-end estimates for the electricity tariffs and low-end estimates for the installation costs.

[5] A low sky temperature contributes to lowering the ambient temperature the same way it draws heat from our PVT collectors.

CRediT authorship contribution statement

Manuel Koch: Writing – original draft, Visualization, Software, Methodology, Investigation, Conceptualization; **Parantapa Sawant:** Writing – review & editing, Supervision, Methodology; **Ralph Eismann:** Funding acquisition, Conceptualization; **Colin N. Jones:** Writing – review & editing, Supervision, Funding acquisition.

Data availability

Input data publicly available. Reference in paper.

Declaration of competing interest

The authors declare that they have no known competing financial interests or personal relationships that could have appeared to influence the work reported in this paper.

References

[1] Enerdata, Residential Buildings: Energy Efficiency & Consumption Evolution in Europe, 2021, https://www.enerdata.net/publications/executive-briefing/households-energy-efficiency.html.
[2] U.S. E.I. Administration, U.S. Energy Facts Explained - consumption and Production, https://www.eia.gov/energyexplained/us-energy-facts/.
[3] U.S. E.I. Administration, Use of Energy in Commercial Buildings in Depth, https://www.eia.gov/energyexplained/use-of-energy/commercial-buildings-in-depth.php.
[4] U.S. E.I. Administration, Use of Energy in Homes, https://www.eia.gov/energyexplained/use-of-energy/homes.php.
[5] B.f. Energie, Energieverbrauch nach Verwendungszweck, https://www.bfe.admin.ch/bfe/de/home/versorgung/statistik-und-geodaten/energiestatistiken/energieverbrauch-nach-verwendungszweck.{html}.
[6] R. Pomeroy, How People Created Ice in the Desert 2,000 Years Ago, 2018, https://www.realclearscience.com/blog/2018/07/09/how_people_created_ice_in_the_desert_2000_years_ago.html.
[7] NASA, The Intervening Atmosphere: tracing the Provenance of a Favorite Landsat Infographic, 2020, https://landsat.gsfc.nasa.gov/article/the-intervening-atmosphere-tracing-the-provenance-of-a-favorite-landsat-infographic/.
[8] A.S.f. Testing, Materials, Standard Extraterrestrial Spectrum Reference E-490-00, 2000, https://www.nrel.gov/grid/solar-resource/spectra-astm-e490.HTML.
[9] G.N. Nwaji, C.A. Okoronkwo, N.V. Ogueke, E.E. Anyanwu, Hybrid solar water heating/nocturnal radiation cooling system I: a review of the progress, prospects and challenges, Energy Build. 198 (2019) 412–430. https://doi.org/10.1016/j.enbuild.2019.06.017
[10] B. Zhao, M. Hu, X. Ao, N. Chen, G. Pei, Radiative cooling: a review of fundamentals, materials, applications, and prospects, Appl. Energy 236 (2019) 489–513. https://doi.org/10.1016/j.apenergy.2018.12.018
[11] D. Zhao, A. Aili, Y. Zhai, S. Xu, G. Tan, X. Yin, R. Yang, Radiative sky cooling: fundamental principles, materials, and applications, Appl. Phys. Rev. 6 (2) (2019) 021306. https://doi.org/10.1063/1.5087281
[12] J. Chen, L. Lu, Development of radiative cooling and its integration with buildings: a comprehensive review, Sol. Energy 212 (2020) 125–151. https://doi.org/10.1016/j.solener.2020.10.013
[13] A. Pirvaram, N. Talebzadeh, S.N. Leung, P.G. O'Brien, Radiative cooling for buildings: a review of techno-Enviro-Economics and life-cycle assessment methods, Renew. Sustain. Energy Rev. 162 (2022) 112415. https://doi.org/10.1016/j.rser.2022.112415
[14] N. Abdelnour, R. Braun, H. Torio, U. Eicker, A simulation-Based study to evaluate the cooling potential of nocturnal radiative cooling systems for residential buildings in egypt, Solar Energy Adv. 3 (2023) 100044. https://doi.org/10.1016/j.seja.2023.100044
[15] S. Suhendri, M. Hu, Y. Dan, Y. Su, B. Zhao, S. Riffat, Building energy-saving potential of a dual-Functional solar heating and radiative cooling system, Energy Build. 303 (2024) 113764. https://doi.org/10.1016/j.enbuild.2023.113764

[16] M. Koch, R. Dott, R. Eismann, Coolshift – cooling of buildings by chiller-Assisted nocturnal radiation and convection, J. Phys. Conf. Ser. 1343 (1) (2019) 012101. https://doi.org/10.1088/1742-6596/1343/1/012101

[17] M. Koch, P. Sawant, R. Eismann, C.N. Jones, Model predictive control for a multi-modal nocturnal radiative cooling system, in: Proceedings of SimBuild Conference 2024, 11 of *IBPSA-USA Building Simulation Conference*, IBPSA-USA, Denver, Colorado, 2024, pp. 778–789. https://publications.ibpsa.org/conference/paper/?id=simbuild2024_2128.

[18] Bundesamt für Umwelt, Belastungsgrenzwerte Für Lärm, 2021, https://www.bafu.admin.ch/bafu/de/home/themen/laerm/fachinformationen/laermbelastung/grenzwerte-fuer-laerm/belastungsgrenzwerte-fuer-laerm.html.

[19] Z. Tian, J.A. Love, A field study of occupant thermal comfort and thermal environments with radiant slab cooling, Build. Environ. 43 (10) (2008) 1658–1670. https://doi.org/10.1016/j.buildenv.2007.10.012

[20] M.A. Hassan, O. Abdelaziz, Best practices and recent advances in hydronic radiant cooling systems – part II: simulation, control, and integration, Energy Build. 224 (2020) 110263. https://doi.org/10.1016/j.enbuild.2020.110263

[21] G. Sastry, P. Rumsey, VAV vs. radiant: side-by-side comparison, ASHRAE J. 56 (2014) 16–24.

[22] M. Killian, M. Kozek, Ten questions concerning model predictive control for energy efficient buildings, Build. Environ. 105 (2016) 403–412. https://doi.org/10.1016/j.buildenv.2016.05.034

[23] T. Hilliard, M. Kavgic, L. Swan, Model predictive control for commercial buildings: trends and opportunities, Adv. Build. Energy Res. 10 (2) (2016) 172–190. https://doi.org/10.1080/17512549.2015.1079240

[24] R. Dott, M. Haller, J. Ruschenburg, F. Ochs, J. Bony, The reference framework for system simulations of the IEA SHC Task 44 / HPP annex 38 part B: buildings and space heat load, 2014. https://doi.org/10.13140/2.1.2221.4727

[25] B. Glück, WärmeÃ¼bergangskoeffizienten an thermisch aktiven BauteiloberflÃ¤chen und der Übergang zu Basiskennlinien fÃ¼r die Wärmestromdichte, gi Gesundeits-Ingenieur 1 (2007) 1–10.

[26] International Organization for Standardization, ISO 6946:2017: Building components and building elements - thermal resistance and thermal transmittance - calculation methods, 2017.

[27] International Organization for Standardization, ISO 9806:2017: Solar-energy - Solar thermal collectors - Test methods, 2017.

[28] U. Eicker, A. Dalibard, Photovoltaic–thermal collectors for night radiative cooling of buildings, Sol. Energy 85 (7) (2011) 1322–1335. https://doi.org/10.1016/j.solener.2011.03.015

[29] N. Fernandez, W. Wang, K.J. Alvine, S. Katipamula, Energy savings potential of radiative cooling technologies, Technical Report PNNL-24904, Pacific Northwest National Lab. (PNNL), Richland, WA (United States), 2015. https://doi.org/10.2172/1234791

[30] Lawrence Berkeley National Laboratory, Modelica Buildings Library: Buildings.BoundaryConditions.SkyTemperature, 2023, (Accessed June 5, 2023), https://simulationresearch.lbl.gov/modelica/releases/v8.0.0/help/Buildings_BoundaryConditions_SkyTemperature.html#Buildings.BoundaryConditions.SkyTemperature.

[31] CARNOT Toolbox des Solar-Institut Jülich, https://www.fh-aachen.de/forschung/institute/sij/carnot.

[32] Climate Calculations: Engineering Reference — EnergyPlus 8.3, https://bigladdersoftware.com/epx/docs/8-3/engineering-reference/climate-calculations.html.

[33] L. Gasser, S. Flück, M. Kleingries, C. Meier, M. Bätschmann, B. Wellig, High efficiency heat pumps for low temperature lift applications, in: 12th IEA Heat Pump Conference, Rotterdam, 2017.

[34] R. Dott, T. Afjei, A. Genkinger, A. Dalibard, D. Carbonell, R. Consul, A. Heinz, M. Haller, A. Witzig, J. Facão, F. Ochs, P. Pärisch, Models of sub-components and validation for the IEA SHC Task 44 / HPP Annex 38 part C: heat pump models, 2014. https://doi.org/10.13140/2.1.2876.8321

[35] EnergyPlus, Weather Data Strasbourg, 2023, (Accessed June 5, 2023) https://energyplus.net/weather-location/europe_wmo_region_6/FRA/FRA_Strasbourg.071900_IWEC.

[36] R. Vilà, L. Rincón, M. Medrano, A. Castell, Potential maps for combined nocturnal radiative cooling and diurnal solar heating applications in europe, Sustain. Energy Technol. Assess. 59 (2023) 103381. https://doi.org/10.1016/j.seta.2023.103381

[37] L. Evangelisti, C. Guattari, F. Asdrubali, On the sky temperature models and their influence on buildings energy performance: a critical review, Energy Build. 183 (2019) 607–625. https://doi.org/10.1016/j.enbuild.2018.11.037

[38] S.F. Fux, A. Ashouri, M.J. Benz, L. Guzzella, EKF Based self-Adaptive thermal model for a passive house, Energy Build. 68 (2014) 811–817. https://doi.org/10.1016/j.enbuild.2012.06.016

[39] Z. Afroz, GM. Shafiullah, T. Urmee, G. Higgins, Modeling techniques used in building HVAC control systems: a review, Renew. Sustain. Energy Rev. 83 (2018) 64–84. https://doi.org/10.1016/j.rser.2017.10.044

[40] L. Di Natale, Y. Lian, E.T. Maddalena, J. Shi, C.N. Jones, Lessons Learned from Data-Driven Building Control Experiments: Contrasting Gaussian Process-based MPC, Bilevel DeePC, and Deep Reinforcement Learning, in: 2022 IEEE 61st Conference on Decision and Control (CDC), 2022, pp. 1111–1117. https://doi.org/10.1109/CDC51059.2022.9992445

[41] Gurobi, The Leader in Decision Intelligence Technology, 2023, (Accessed June 5, 2023) https://www.gurobi.com/.

[42] S.I.-u. Architektenverein, Norm SIA 180:2014: Wärmeschutz, Feuchteschutz und Raumklima in Gebäuden, 2014.

[43] DHWcalc Download, https://www.uni-kassel.de/maschinenbau/institute/thermische-energietechnik/fachgebiete/solar-und-anlagentechnik/downloads.

[44] Intel Core I9-11900K @ 3.50GHz vs ARM Cortex-A76 4 Core 2400 MHz [Cpubenchmark.Net] by PassMark Software, https://www.cpubenchmark.net/compare/3904vs5743/Intel-i9-11900K-vs-ARM-Cortex-A76-4-Core-2400-MHz.

[45] EnergyPlus, https://energyplus.net/.

[46] M. Wetter, W. Zou, T.S. Nouidui, X. Pang, Modelica buildings library, J. Build. Perform. Simul. 7 (4) (2014) 253–270. https://doi.org/10.1080/19401493.2013.765506

[47] G. Serale, M. Fiorentini, A. Capozzoli, D. Bernardini, A. Bemporad, Model predictive control (MPC) for enhancing building and HVAC system energy efficiency: problem formulation, applications and opportunities, Energies 11 (3) (2018) 631. https://doi.org/10.3390/en11030631

[48] J. Drgoňa, J. Arroyo, I. Cupeiro Figueroa, D. Blum, K. Arendt, D. Kim, E.P. Ollé, J. Oravec, M. Wetter, D.L. Vrabie, L. Helsen, All you need to know about model predictive control for buildings, Annu. Rev. Control (2020). https://doi.org/10.1016/j.arcontrol.2020.09.001

[49] S. Taheri, P. Hosseini, A. Razban, Model predictive control of heating, ventilation, and air conditioning (HVAC) systems: a state-of-the-Art review, J. Build. Eng. 60 (2022) 105067. https://doi.org/10.1016/j.jobe.2022.105067

[50] L. Gelažanskas, K.A.A. Gamage, Forecasting hot water consumption in residential houses, Energies 8 (11) (2015) 12702–12717. https://doi.org/10.3390/en81112336

[51] A. Lomet, F. Suard, D. Chèze, Statistical modeling for real domestic hot water consumption forecasting, Energy Procedia 70 (2015) 379–387. https://doi.org/10.1016/j.egypro.2015.02.138

[52] F. Oldewurtel, C.N. Jones, A. Parisio, M. Morari, Stochastic model predictive control for building climate control, IEEE Trans. Control Syst. Technol. 22 (3) (2014) 1198–1205. https://doi.org/10.1109/TCST.2013.2272178

[53] E.T. Maddalena, S.A. Müller, R.M. dos Santos, C. Salzmann, C.N. Jones, Experimental data-driven model predictive control of a hospital HVAC system during regular use, Energy Build. 271 (2022) 112316. https://doi.org/10.1016/j.enbuild.2022.112316

[54] Levelized Cost of Energy+, https://www.lazard.com/research-insights/levelized-cost-of-energyplus/.

[55] Themenheft 59: Modulare Gebäudetechnik – Faktor.ch, https://faktor.ch/produkt/themenheft-59-modulare-gebaeudetechnik/.